# EFFECTS OF CENTRAL AND DENSITY-DEPENDENT TERMS OF THE SKYRME INTERACTION ON NEUTRON ELASTIC SCATTERING OBSERVABLES

H. Cong Quang[a,b†], N. Hoang Tung[c,d], Vinh N.T. Pham[e]
Meng-Hock Koh[f], N. Quang Hung[g,h], N. Ngoc Duy[i]
K. Mizuyama[j,g], T.V. Nhan Hao[a,b‡]

[a]Faculty of Physics, University of Education, Hue University
34 Le Loi Street, Hue City, Vietnam
[b]Center for Theoretical and Computational Physics, University of Education
Hue University, 34 Le Loi Street, Hue City, Vietnam
[c]Department of Nuclear Physics and Nuclear Engineering, Faculty of Physics and Engineering Physics, University of Science, Ho Chi Minh City, Vietnam
[d]Vietnam National University, Ho Chi Minh City, Vietnam
[e]Department of Physics, Ho Chi Minh City University of Education
Ho Chi Minh City 700000, Vietnam
[f]Department of Physics, Faculty of Science, Universiti Teknologi Malaysia
81310 Johor Bahru, Johor, Malaysia
[g]Institute of Fundamental and Applied Sciences, Duy Tan University
Ho Chi Minh City 700000, Vietnam
[h]Faculty of Natural Sciences, Duy Tan University, Da Nang City 550000, Vietnam
[i]Institute of Postgraduate, Van Lang University
Ho Chi Minh City 700000, Vietnam
[j]Institute of Research and Development, Duy Tan University
Da Nang 550000, Vietnam

*Received 13 April 2022, accepted 9 June 2022,*
*published online 29 June 2022*

In this paper, we analyze the role of central ($t_0$) and density-dependent ($t_3$) terms of the effective Skyrme interaction on the imaginary part of the optical potential, angular distributions, and analyzing powers of the low-energy neutron elastic scattering on a series of doubly closed shell nuclei in the framework of self-consistent mean-field approach and beyond. The central term is the leading term of the effective interaction, while the density-dependent term is well known to be an effective way to simulate the three-body interaction. To do it, the microscopic optical potential has been generated from the particle vibration coupling on top of the random-phase

† huynhcongquang@dhsphue.edu.vn
‡ Corresponding author: tvnhao@hueuni.edu.vn

approximation collective states built from the particle–hole excitations on a mean-field calculation. It has been found that the contributions of $(t_0, t_3)$ terms are dominant on the surface and in the interior of the absorption part. The effects of $t_0$ term are the strongest among other terms. The obtained results show that, if the central and density-dependent terms are taken into account, the agreement on angular distributions is significantly improved, especially at the forward scattering angles. The two terms were also found to have strong yet unsystematic effects on analyzing power.

DOI:10.5506/APhysPolB.53.7-A4

Microscopic optical potential (MOP) is expected to be a useful tool to study exotic nuclei lying far from the stability island. There has been impressive progress over the last decade to develop this kind of potential based on the nuclear many-body theories [1, 2]. At energy lower than 50 MeV where the nuclear structure effects become important, the MOP based on nuclear structure models has successfully unified the nuclear structure and nuclear reactions in terms of the $n$–$A$ elastic scattering. Therefore, the elastic scattering observables have been directly connected with the underlying nucleon–nucleon ($NN$) effective phenomenological interactions [3–6]. The effective interactions (mostly the finite-range Gogny and zero-range Skyrme interactions) have been initially designed for nuclear structure calculations. Within the framework of self-consistent mean-field approach and beyond, these effective Skyrme and Gogny interactions (with about 10 parameters) provide a rather good description of the binding energies, charge r.ms. radii, and excited states of finite nuclei as well as the properties of nuclear matter around its saturation density $\rho_0$. In nuclear reactions, these effective interactions have been successfully used to describe the nucleon elastic scattering by $^{208}$Pb [3], neutron elastic scattering by $^{16}$O[4], proton inelastic scattering by $^{24}$O [7], nucleon elastic scattering by $^{40}$Ca and $^{48}$Ca [5, 8, 9], and nucleon elastic scattering by $^{16}$O, $^{40}$Ca, $^{48}$Ca, and $^{208}$Pb [6, 10–12]. It is interesting to note that the MOPs at the positive and negative energies are naturally and consistently connected since these potentials are based on the self-energy extracted from the mass operator in the framework of many-body Green function method.

However, the precision of the mentioned MOPs is not high compared to the phenomenological one due to some deviations from the experimental data at backward angles. This is, indeed, an intricate problem which requires an intensive analysis of the sensitivity of nuclear reaction observables on each component of the effective Skyrme interaction. Such an analysis is particularly important to significantly improve and/or build a new generation of optical potential. Recently, we have reported the first intensive analysis of the effects of velocity-dependent $(t_1, t_2)$ and spin-orbit terms on neutron elastic scattering observables at low energies within a fully self-consistent particle-vibration coupling built on top of the RPA excited states [12]. In the present paper, the above model has been further applied to analyze the role of central and density-dependent interactions on the neutron elastic scatterings of doubly closed-shell targets.

Below, we show the conventional non-relativistic zero-range density and momentum-dependent phenomenological Skyrme interaction

$$
\begin{aligned}
V_{\text{Skyrme}}(\boldsymbol{r}_1,\boldsymbol{r}_2) &= t_0(1+x_0P^\sigma)\delta(\boldsymbol{r}) && t_0 \text{ term or central term} \\
&+ \tfrac{1}{2}t_1(1+x_1P^\sigma)\left[\boldsymbol{k}'^2\delta(\boldsymbol{r})+\delta(\boldsymbol{r})\boldsymbol{k}^2\right] && \\
&+ t_2(1+x_2P^\sigma)\boldsymbol{k}'\cdot\delta(\boldsymbol{r})\boldsymbol{k} && t_1,t_2 \text{ term or velocity-dependent term} \\
&+ iW_0(\vec{\sigma}_1+\vec{\sigma}_2)\cdot[\boldsymbol{k}'\times\delta(\boldsymbol{r})\boldsymbol{k}] && W_0 \text{ term or spin-orbit term} \\
&+ \tfrac{1}{6}t_3(1+x_3P^\sigma)\rho^\alpha(\boldsymbol{R})\delta(\boldsymbol{r}) && t_3 \text{ term or density-dependent term}\,,
\end{aligned}
\tag{1}
$$

where $\boldsymbol{r} = \boldsymbol{r}_1 - \boldsymbol{r}_2$, $\boldsymbol{R} = \frac{1}{2}(\boldsymbol{r}_1 + \boldsymbol{r}_2)$, $\boldsymbol{k} = \frac{1}{2i}(\vec{\nabla}_1 - \vec{\nabla}_2)$, $\boldsymbol{k}'$ is the hermitian conjugate of $\boldsymbol{k}$ (acting on the left), $P^\sigma = \frac{1}{2}(1 + \vec{\sigma}_1 \cdot \vec{\sigma}_2)$ is the spin-exchange operator, and $\rho$ is the total nucleon density. The parameters $t_0, t_1, t_2, t_3, W_0, \alpha, x_0, x_1, x_2, x_3$ are obtained by fitting to the experimental data.

To investigate the role of each term of the effective interaction on the nuclear reactions observables, the effective interaction must be fully and consistently used in the whole process to generate the MOP. Until now, there are two fully self-consistent calculations by Blanchon *et al.* [5] (with Gogny interaction) and Nhan Hao *et al.* [6] (with Skyrme interaction). We will only sketch here the major points of our MOP. According to Refs. [6, 10–12], the MOP is given as

$$
V_{\text{opt}} = V_{\text{HF}} + \Delta\Sigma(\omega)\,, \tag{2}
$$

where

$$
\Delta\Sigma(\omega) = \Sigma(\omega) - \tfrac{1}{2}\Sigma^{(2)}(\omega)\,. \tag{3}
$$

In Eqs. (2) and (3), $V_{\text{HF}}$ is a static, real, local, and energy-independent Skyrme–Hartree–Fock mean field. The first order, $\Sigma(\omega)$, is the contribution from the particle-vibration coupling calculated as in Refs. [6, 14, 15]. This dynamical potential is non-local, complex, and energy-dependent. The symbol $\omega$ is the nucleon incident energy. The second order potential, $\Sigma^{(2)}(\omega)$, is taken into account to treat the issue of the Pauli principle correction. The $NN$ effective phenomenological interaction SLy5 [13] has been adopted. Note that all parameters are fixed and are the same as in Refs. [6, 10–12].

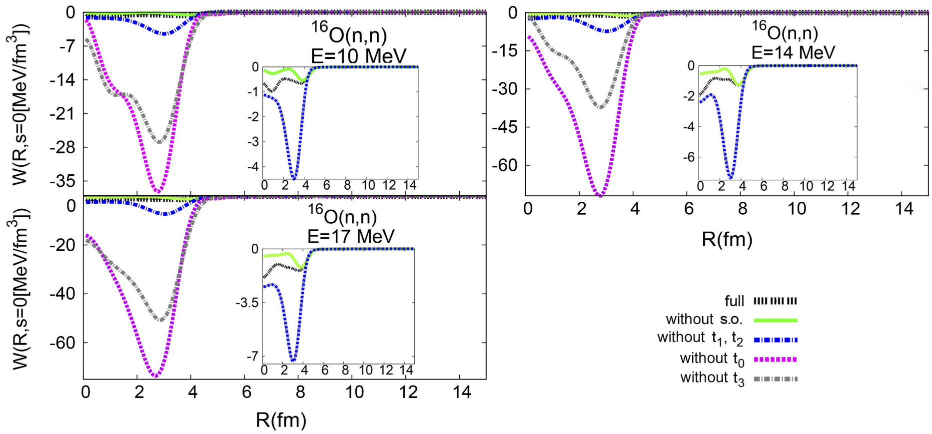


Fig. 1. The calculated $W(R, s = 0)$ for neutron elastic scattering by $^{16}$O at low incident energies. The linepoints curve shows the calculation with the full effective SLy5 Skyrme interaction. The green curve shows the calculation without spin-orbit term. The blue line shows the calculation without $t_1, t_2$ term. The purple line (gray line) shows the calculation without $t_0$ ($t_3$) term, respectively. The calculated results for $t_1, t_2, W_0$ using the same MOPs are adapted from [12].

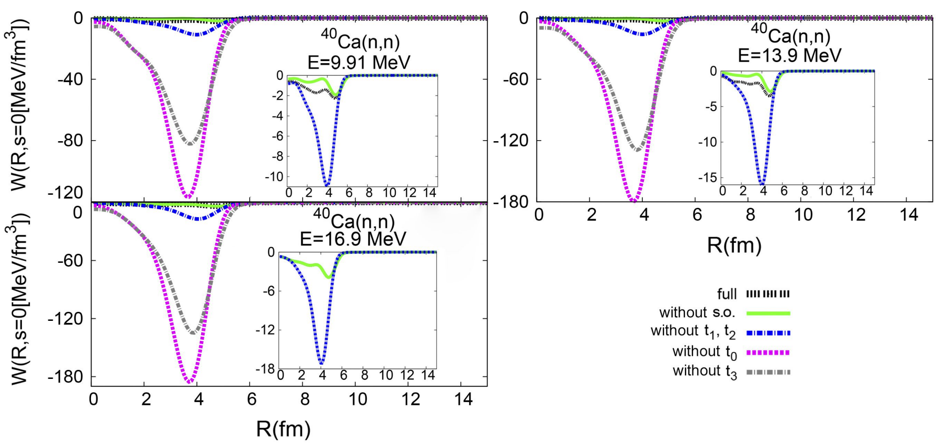


Fig. 2. The calculated $W(R, s = 0)$ for neutron elastic scattering by $^{40}$Ca at low incident energies. The linepoints curve shows the calculation with the full effective SLy5 Skyrme interaction. The green curve shows the calculation without spin-orbit term. The blue line shows the calculation without $t_1, t_2$ term. The purple line (gray line) shows the calculation without $t_0$ ($t_3$) term, respectively. The calculated results for $t_1, t_2, W_0$ using the same MOPs are adapted from [12].

To see the effects of each term on the absorption, we consider the diagonal contributions $W(R, s = 0)$ of the imaginary part, where $W(R, s) = \sum_{lj} \frac{2j+1}{4\pi} \mathrm{Im}\Delta\Sigma_{lj}(r, r', \omega)$, with $R = \frac{1}{2}(r + r')$ corresponding to the radius and shape of $\mathrm{Im}\Delta\Sigma$, and $s = r - r'$ being its non-locality. Figures 1, 2, 3, and 4 show the calculations of $W(R, s = 0)$ with and without $t_0$, $t_3$, $t_1, t_2$, and $W_0$ terms for neutron elastic scattering by $^{16}$O, $^{40}$Ca, $^{48}$Ca, and $^{208}$Pb at different incident energies.

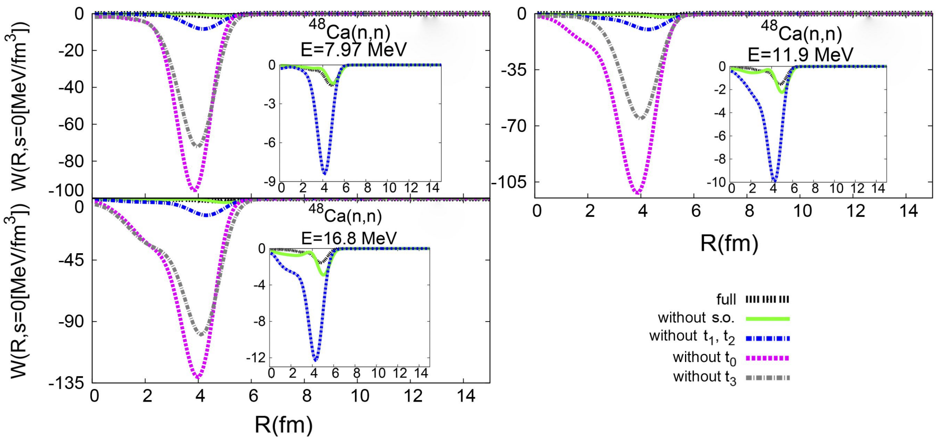


Fig. 3. The calculated $W(R, s = 0)$ for neutron elastic scattering by $^{48}$Ca at low incident energies. The linepoints curve shows the calculation with the full effective SLy5 Skyrme interaction. The green curve shows the calculation without spin-orbit term. The blue line shows the calculation without $t_1, t_2$ term. The purple line (gray line) shows the calculation without $t_0$ ($t_3$) term, respectively. The calculated results for $t_1, t_2, W_0$ using the same MOPs are adapted from [12].

First, the obtained results show that on the surface and also in the interior, the effects of $t_0, t_3$ terms are dominant compared with other terms. The inclusion of $t_0, t_3$ terms strongly reduces the absorption of the imaginary part which means that these terms strongly decrease the coupling to collective states. The effects of $t_0$ interaction are always larger than that of $t_3$ interaction. These results show, in nuclear reactions, not only the leading role of $t_0$ term (the major part of the nucleon–nucleon effective interaction) but also the important role of the $t_3$ term which somehow simulates the 3-body interaction. Figures 5, 6, 7, and 8 show the angular distributions for neutron elastic scattering by $^{16}$O, $^{40}$Ca, $^{48}$Ca, and $^{208}$Pb with and without $t_0$, $t_3$, $t_1, t_2$, and $W_0$ terms at different incident energies. For all nuclei at all incident energies, the obtained results show that the $t_0, t_3$ terms play an important role (especially on the forward scattering angles) since the inclusion of these terms strongly improves the agreement of angular distributions with experimental data. There is a systematic agreement between the calculations and the experimental data for the angular distributions at scattering angles smaller than 40°. It shows that the surface properties of the MOP have been very well treated. The agreement gets worse with increasing the scattering angles, especially at backward angles. This disagreement is an intricate problem (it also happens for previous works for both POP [16] and MOP [17]) due to the lack of absorption in the interior region of the imaginary part of MOP. The main reason could be the limit of the zero-range effective Skyrme interaction since it is designed firstly for the nuclear structure.

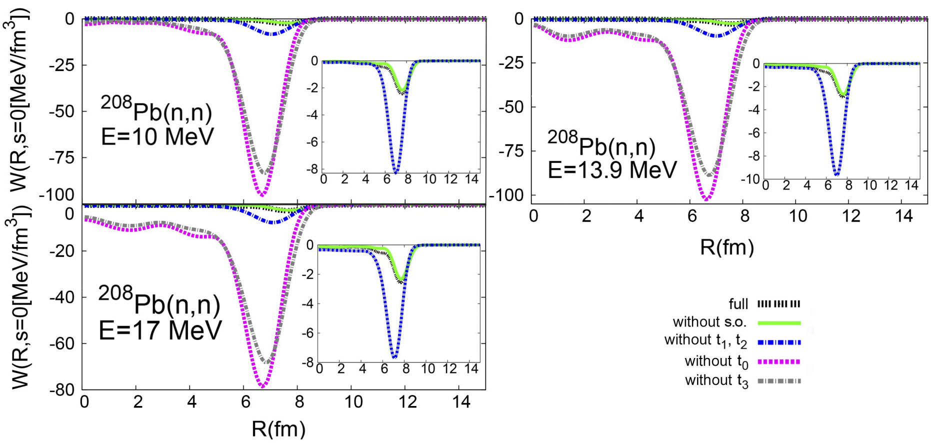


Fig. 4. The calculated $W(R, s = 0)$ for neutron elastic scattering by $^{208}$Pb at low incident energies. The linepoints curve shows the calculation with the full effective SLy5 Skyrme interaction. The green curve shows the calculation without spin-orbit term. The blue line shows the calculation without $t_1, t_2$ term. The purple line (gray line) shows the calculation without $t_0$ ($t_3$) term, respectively. The calculated results for $t_1, t_2, W_0$ using the same MOPs are adapted from [12].

In Figs. 9, 10, 11, and 12, we compare the experimental data with the analyzing powers obtained within the present MOP for neutron elastic scattering by $^{16}$O, $^{40}$Ca, $^{48}$Ca, and $^{208}$Pb with and without the $t_0$, $t_3$, $t_1, t_2$, and $W_0$ terms at different incident energies. These results show that the $t_0, t_3$ terms have strong but unsystematic effects on analyzing powers. For example, the inclusion of $t_0, t_3$ terms for $^{48}$Ca at 7.97 MeV improves the agreement with experimental data but it becomes worse for $^{16}$O at 10 MeV. In general, the agreement between the calculation and experimental data is poor. It shows that, in our model, the spin-orbit interaction of the effective Skyrme interaction is not well adapted to describe the polarization observables.

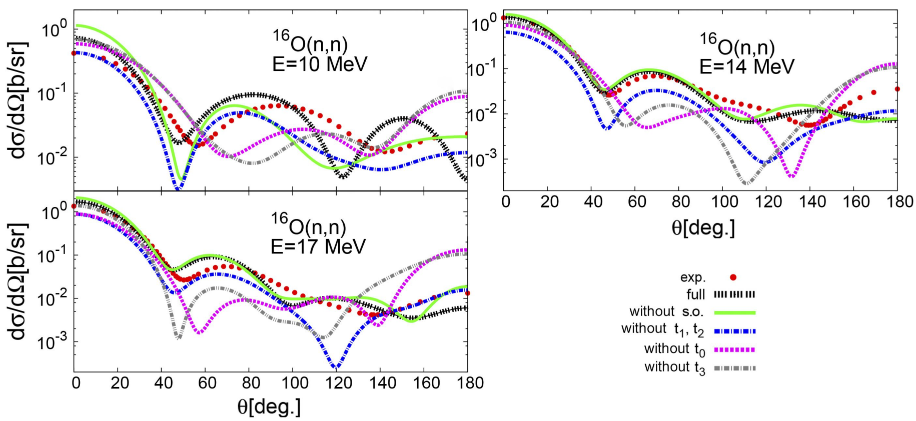


Fig. 5. Angular distributions of neutron elastic scattering by $^{16}$O at low incident energies. The linepoints curve shows the calculation with the full effective SLy5 Skyrme interaction. The green curve shows the calculation without spin-orbit term. The blue line shows the calculation without $t_1, t_2$ term. The purple line (gray line) shows the calculation without $t_0$ ($t_3$) term, respectively. The experimental data points are taken from [18]. The calculated results for $t_1, t_2, W_0$ using the same MOPs are adapted from [12].

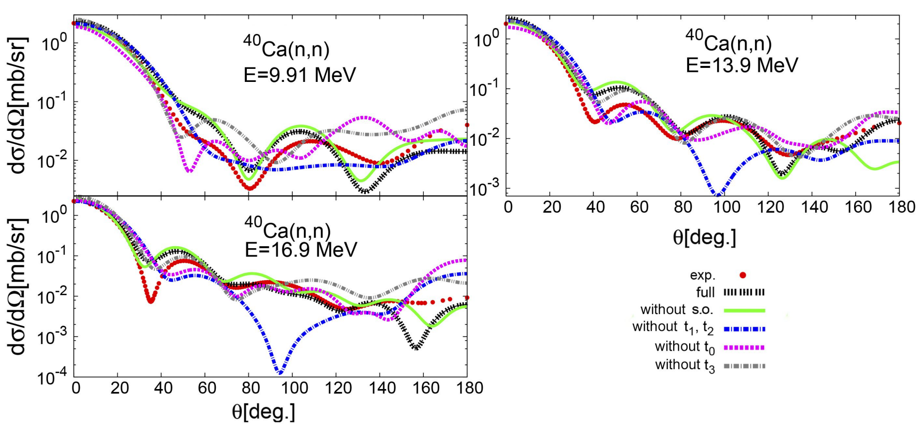


Fig. 6. Angular distributions of neutron elastic scattering by $^{40}$Ca at low incident energies. The linepoints curve shows the calculation with the full effective SLy5 Skyrme interaction. The green curve shows the calculation without spin-orbit term. The blue line shows the calculation without $t_1, t_2$ term. The purple line (gray line) shows the calculation without $t_0$ ($t_3$) term, respectively. The experimental data points are taken from [18]. The calculated results for $t_1, t_2, W_0$ using the same MOPs are adapted from [12].

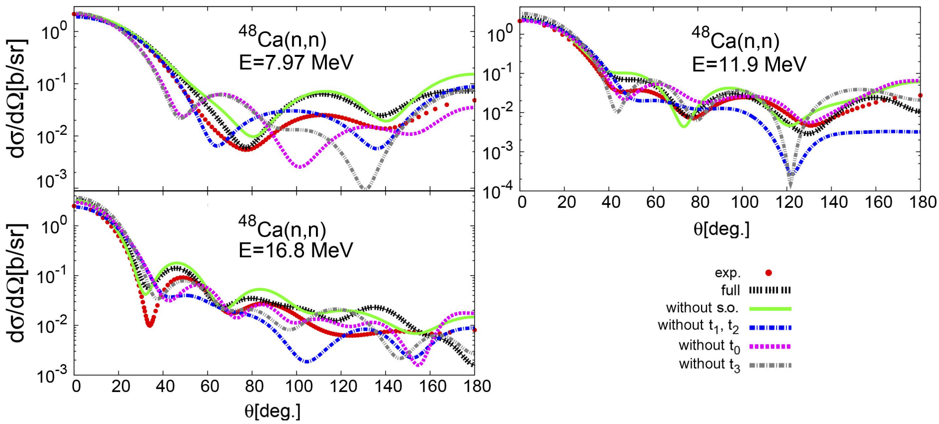


Fig. 7. Angular distributions of neutron elastic scattering by $^{48}$Ca at low incident energies. The linepoints curve shows the calculation with the full effective SLy5 Skyrme interaction. The green curve shows the calculation without spin-orbit term. The blue line shows the calculation without $t_1, t_2$ term. The purple line (gray line) shows the calculation without $t_0$ ($t_3$) term, respectively. The experimental data points are taken from [18]. The calculated results for $t_1, t_2, W_0$ using the same MOPs are adapted from [12].

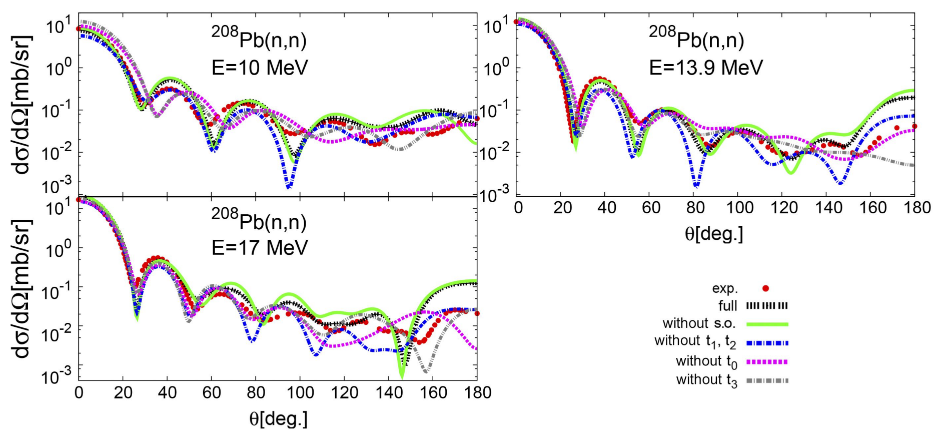


Fig. 8. Angular distributions of neutron elastic scattering by $^{208}$Pb at low incident energies. The linepoints curve shows the calculation with the full effective SLy5 Skyrme interaction. The green curve shows the calculation without spin-orbit term. The blue line shows the calculation without $t_1, t_2$ term. The purple line (gray line) shows the calculation without $t_0$ ($t_3$) term, respectively. The experimental data points are taken from [18]. The calculated results for $t_1, t_2, W_0$ using the same MOPs are adapted from [12].

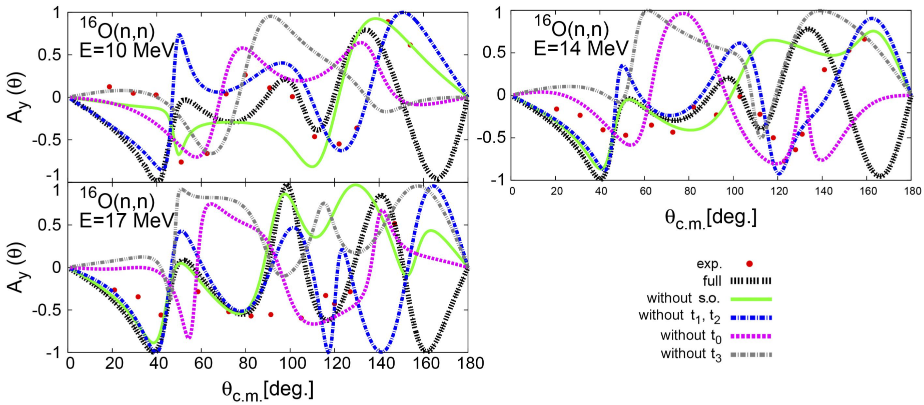


Fig. 9. Analyzing power of neutron elastic scattering by $^{16}$O at low incident energies. The linepoints curve shows the calculation with the full effective SLy5 Skyrme interaction. The green curve shows the calculation without spin-orbit term. The blue line shows the calculation without $t_1, t_2$ term. The purple line (gray line) shows the calculation without $t_0$ ($t_3$) term, respectively. The experimental data points are taken from [18]. The calculated results for $t_1, t_2, W_0$ using the same MOPs are adapted from [12].

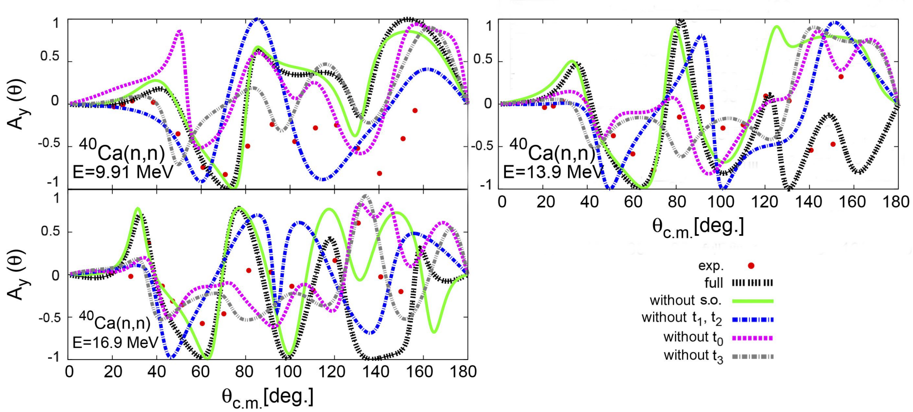


Fig. 10. Analyzing power of neutron elastic scattering by $^{40}$Ca at low incident energies. The linepoints curve shows the calculation with the full effective SLy5 Skyrme interaction. The green curve shows the calculation without spin-orbit term. The blue line shows the calculation without $t_1, t_2$ term. The purple line (gray line) shows the calculation without $t_0$ ($t_3$) term, respectively. The experimental data points are taken from [18]. The calculated results for $t_1, t_2, W_0$ using the same MOPs are adapted from [12].

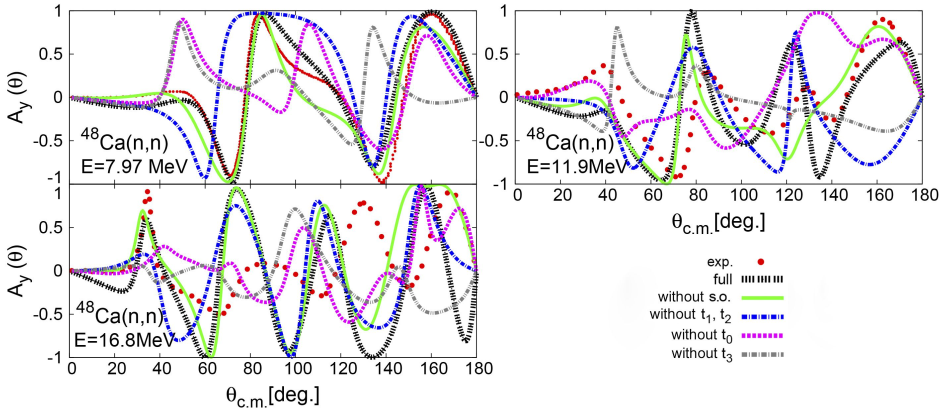


Fig. 11. Analyzing power of neutron elastic scattering by $^{48}$Ca at low incident energies. The linepoints curve shows the calculation with the full effective SLy5 Skyrme interaction. The green curve shows the calculation without spin-orbit term. The blue line shows the calculation without $t_1, t_2$ term. The purple line (gray line) shows the calculation without $t_0$ ($t_3$) term, respectively. The experimental data points are taken from [18]. The calculated results for $t_1, t_2, W_0$ using the same MOPs are adapted from [12].

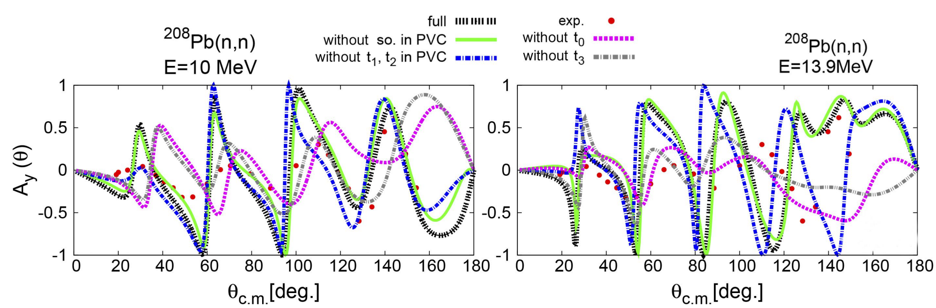


Fig. 12. Analyzing power of neutron elastic scattering by $^{208}$Pb at low incident energies. The linepoints curve shows the calculation with the full effective SLy5 Skyrme interaction. The green curve shows the calculation without spin-orbit term. The blue line shows the calculation without $t_1, t_2$ term. The purple line (gray line) shows the calculation without the $t_0$ ($t_3$) term, respectively. The experimental data points are taken from [18]. The calculated results for $t_1, t_2, W_0$ using the same MOPs are adapted from [12].

This work is a further step of our project devoted to get (as much as possible) the nuclear structure information directly and microsopically from the analysis of scattering experimental data. The obtained results show that it is very hard (even impossible) to have a very high precision global microscopic optical potential generated directly from the existing $NN$ effective interaction. We plan, in our long-term goal, to build a new generation of optical potential which could be the combination between the phenomenological and microscopic optical potential. Therefore, the obtained information plays an important role and helps us to build the framework for new optical potentials. For the next step, we will investigate the sensitivity of the nuclear reaction observables on each parameter of the effective Skyrme interaction. In the light of this work, the elastic scattering observables could be the new constraint to get the new sets of parameters for the effective phenomenological Skyrme-type interactions which could simultaneously describe the nuclear structure and nuclear reactions at low-energy.

This research is funded by the University of Education, Hue University under grant No. T. 20-TN.SV-02. M.H.K. would like to acknowledge the Ministry of Education of Malaysia for the financial support through the Fundamental Research Grant Scheme FRGS/1/2018/ST/G02/UTM/02/6 and UTM R.J130000.7854.5F028. T.V.N.H. and N.Q.H. acknowledge the partial support by the National Foundation for Science and Technology Development under grant No. 103.04-2019.371. This work was partially supported by the Hue University under the Core Research Program, grant No. NCM.DHH.2018.09.

## REFERENCES

[1] W.H. Dickhoff, R.J. Charity, «Recent developments for the optical model of nuclei», *Prog. Part. Nucl. Phys.* **105**, 252 (2019).

[2] A. Bonaccorso, «Direct reaction theories for exotic nuclei: An introduction via semi-classical methods», *Prog. Part. Nucl. Phys.* **101**, 1 (2018).

[3] V. Bernard, N. Van Giai, «Microscopic optical potential for $^{208}$Pb in the nuclear structure approach», *Nucl. Phys. A* **327**, 397 (1979).

[4] K. Mizuyama, K. Ogata, «Self-consistent microscopic description of neutron scattering by $^{16}$O based on the continuum particle-vibration coupling method», *Phys. Rev. C* **86**, 041603(R) (2012).

[5] G. Blanchon, M. Dupuis, H.F. Arellano, N. Vinh Mau, «Microscopic positive-energy potential based on the Gogny interaction», *Phys. Rev. C* **91**, 014612 (2015).

[6] T.V. Nhan Hao, Bui Minh Loc, Nguyen Hoang Phuc, «Low-energy nucleon–nucleus scattering within the energy density functional approach», *Phys. Rev. C* **92**, 014605 (2015).

[7] K. Mizuyama, K.Ogata, «Low-lying excited states of $^{24}$O investigated by a self-consistent microscopic description of proton inelastic scattering», *Phys. Rev. C* **89**, 034620 (2014).

[8] G. Blanchon, M. Dupuis, R.N. Bernard, H.F. Arellano, «Asymmetry dependence of Gogny-based optical potential», *Eur. Phys. J. A* **53**, 88 (2017).

[9] G. Blanchon, M. Dupuis, H.F. Arellano, «Prospective study on microscopic potential with Gogny interaction», *Eur. Phys. J. A* **51**, 165 (2015).

[10] T.V. Nhan Hao *et al.*, «Microscopic optical potential obtained from energy-density-functional approach for neutron–nucleus elastic scattering», *Int. J. Mod. Phys. E* **27**, 1850052 (2018).

[11] N. Hoang Tung, N. Nhu Le, V.N.T. Pham, T.V. Nhan Hao, «Microscopic Optical Model Analysis of Proton–Nucleus Elastic Scattering at Low Energy», *Acta Phys. Pol. B* **51**, 1929 (2020).

[12] N. Hoang Tung *et al.*, «Effects of velocity-dependent and spin-orbit terms of the Skyrme interaction on neutron elastic scattering observables», *Phys. Rev. C* **102**, 034608 (2020).

[13] E. Chabanat *et al.*, «A Skyrme parametrization from subnuclear to neutron star densities Part II. Nuclei far from stabilities», *Nucl. Phys. A* **635**, 231 (1998).

[14] G. Colò, H. Sagawa, P.F. Bortignon, «Effect of particle-vibration coupling on single-particle states: A consistent study within the Skyrme framework», *Phys. Rev. C* **82**, 064307 (2010).

[15] Li-Gang Cao, G. Colò, H. Sagawa, P. F. Bortignon, «Properties of single-particle states in a fully self-consistent particle-vibration coupling approach», *Phys. Rev. C* **89**, 044314 (2014).

[16] A.J. Koning, J.P. Delaroche, «Local and global nucleon optical models from 1 keV to 200 MeV», *Nucl. Phys. A* **713**, 231 (2003).

[17] E. Bauge, J.P. Delaroche, M. Girod, «Lane-consistent, semimicroscopic nucleon–nucleus optical model», *Phys. Rev. C* **63**, 024607 (2001).

[18] Experimental data taken from the National Nuclear Data Center, Brookhaven National Laboratory Online Data Service, `http://www.nndc.bnl.gov/ensdf/`.